Max Weigler[a], Martin Brodrecht[a], Hergen Breitzke, Felix Dietrich, Matthias Sattig, Gerd Buntkowsky* and Michael Vogel*

^{2}H NMR Studies on Water Dynamics in Functionalized Mesoporous Silica

https://doi.org/10.1515/zpch-2017-1034
Received September 14, 2017; accepted November 9, 2017

Abstract: Mesoporous silica MCM-41 is prepared, for which the inner surfaces are modified by 3-(aminopropyl)triethoxysilane (APTES) in a controlled manner. Nitrogen gas adsorpition yields a pore diameter of 2.2 nm for the APTES functionalized MCM-41. ^{2}H nuclear magnetic resonance (NMR) and broadband dielectric spectroscopy (BDS) provide detailed and consistent insights into the temperature-dependent reorientation dynamics of water in this confinement. We find that a liquid water species becomes accompanied by a solid water species when cooling through ~210 K, as indicated by an onset of bimodal ^{2}H spin-lattice relaxation. The reorientation of the liquid water species is governed by pronounced dynamical heterogeneity in the whole temperature range. Its temperature dependence shows a mild dynamic crossover when the solid water species emerges and, hence, the volume accessible to the liquid water species further shrinks. Therefore, we attribute this variation in the temperature dependence to a change from bulk-like behavior towards interface-dominated dynamics. Below this dynamic crossover, ^{2}H line-shape and stimulted-echo studies show that water reorientation becomes anisotropic upon cooling, suggesting that these NMR approaches, but also BDS measurements do no longer probe the structural (α) relaxation, but rather a secondary (β) relaxation of water at sufficiently low temperatures. Then, another dynamic crossover at ~180 K can be rationalized in terms of a change of the temperature dependence of the β relaxation in response to a glassy freezing of the α relaxation of confined water. Comparing these results for APTES

[a]**Max Weigler and Martin Brodrecht:** These authors contributed equally to this work.
***Corresponding authors: Gerd Buntkowsky,** Eduard-Zintl-Institut für Anorganische unf Physikalische Chemie, Technische Universität Darmstadt, Alarich-Weiss-Str. 8, 64287 Darmstadt, Germany, e-mail: gerd.buntkowsky@chemie.tu-darmstadt.de; and
Michael Vogel, Institut für Festkörperphysik, Technische Universität Darmstadt, Hochschulstr. 6, 64289 Darmstadt, Germany, e-mail: michael.vogel@physik.tu-darmstadt.de
Max Weigler, Felix Dietrich and Matthias Sattig: Institut für Festkörperphysik, Technische Universität Darmstadt, Hochschulstr. 6, 64289 Darmstadt, Germany
Martin Brodrecht and Hergen Breitzke: Eduard-Zintl-Institut für Anorganische unf Physikalische Chemie, Technische Universität Darmstadt, Alarich-Weiss-Str. 8, 64287 Darmstadt, Germany

modied MCM-41 with previous findings for mesoporous silica with various pore diameters, we obtain valuable information about the dependence of water dynamics in restricted geometries on the size of the nanoscopic confinements and the properties of the inner surfaces.

Keywords: confined water; ^{2}H NMR; mesoporous silica.

1 Introduction

In many situations, water is found in nanoscopic confinements. The properties of water under such restraints differ, in general, from that in the bulk [1–4]. A prominent example is the lowering of the freezing point in restricted geometries, which depends on the size and hydroaffinity of the confinement [5–7]. Therefore, it is of major importance to strive for a comprehensive characterization of the properties of water in various environments. Here, we focus on the dynamics of confined water, which is the key to an understanding of biological functions [8] or an optimization of technological processes, e.g. nanofluidics applications.

Despite massive research efforts, the temperature-dependent dynamics of confined water is still a subject of controversial scientific debate [4]. While there appears to be consensus that confined water shows dynamical crossovers in the viscous regime, the origin and interpretation of these phenomena are vigorously disputed. Some authors argued that a transition from fragile (non-Arrhenius) to strong (Arrhenius) behavior occurs [9], which is related to a liquid-liquid phase transition of bulk water [10]. Other workers attributed changes in the temperature dependence to a crossover from structural (α) to secondary (β) relaxation [11, 12]. Some of us conjectured that a dynamic crossover is related to a reduction of the accessible volume during partial freezing, resulting in a transition from bulk-like to interface-dominated water dynamics [13–15].

Many of these studies exploited that tailor-made confinements are available from mesoporous silica, which show cylindrical pores of defined and adjustable diameter. Aiming at a use of confined water as a model of bulk water, which cannot be investigated in the 'no man's land' (~150–235 K) due to immediate crystallization, silica pores with diameters of ~2 nm were frequently used to suppress crystallization of water to a large extent, but, at the same time, avoid confinement effects as far as possible. In general, it is, however, desirable to gain a broad understanding of water dynamics under different confinement conditions. For this purpose, it is advisable to compare water dynamics in confinements with various sizes and surfaces.

Having addressed the size aspect in a previous study [14], we investigate the role of the inner surfaces in this contribution. Specifically, we compare water dynamics in modified and unmodified MCM-41 of comparable pore diameter. For the modification of the inner surfaces, in particular, of their hydrophilicity, we link 3-(aminopropyl)triethoxysilane (APTES) to the silanol groups on the inner surfaces. The obtained functionalized mesosoprous material, which will be denoted MCM-41 APTES in the following, has a pore diameter of 2.2 nm, comparable to native MCM-41 C10 with a pore diameter of 2.1 nm. Therefore, comparison of water motion in these modified and unmodified MCM-41 matrices allows us to ascertain surface effects largely undisturbed by size effects.

To study the dynamical behavior of confined water in broad temperature ranges, we apply various methods of ^{2}H nuclear magnetic resonance (NMR) together with broadband dielectric spetroscopy (BDS). Specifically, we combine ^{2}H spin-lattice relaxation (SLR), line-shape (LS), and stimulated-echo (STE) measurements. This approach allows us to determine both the rates and the mechanisms of water dynamics in a broad dynamic range. To gain insights into the dependence of the dynamics of confined water on the properties of the confining walls, the outcome of these NMR and BDS experiments on MCM-41 APTES are compared with the results of previous studies on MCM-41 C10 [13, 16].

2 ^{2}H NMR background

^{2}H NMR is sensitive to molecular reorientations. It probes the first order quadrupolar interaction between the electric quadrupole moment of the deuterons and the electric field gradient at their sites, which results from the anisotropic charge distribution of the chemical bonds. In detail, the contribution of the quadrupolar interaction to the resonance frequency is given by [17]:

$$\omega_Q = \pm\frac{\delta}{2}(3\cos^2\theta - 1 - \eta\sin^2\theta\cos(2\phi)) \tag{1}$$

Here, the ± signs correspond to the two allowed transitions between the three Zeeman levels of the deuteron. The angles θ and ϕ describe the orientation of the quadrupolar coupling tensor with respect to the external magnetic field $\boldsymbol{B_0}$. Moreover, δ and η denote the anisotropy and asymmetry parameters of this tensor, respectively.

For D_2O, the anisotropy parameter amounts to $\delta \approx 2\pi \cdot 161$ kHz, corresponding to a quadrupolar coupling constant of $2\pi \cdot 215$ kHz, and the asymmetry parameter has a small value of $\eta \approx 0.1$ [13, 14]. Hence, to a good approximation,

the quadrupolar coupling tensor is axially symmetric with a principal z axis pointing along the direction of the O–D bond. Consequently, the fluctuations of the quadrupolar frequencies $\omega_Q(t)$ reflect the reorientations of the O–D bonds. Neglecting the minor anisotropy of the tensor, these fluctuations provide access to the correlation function $F_2(t)$ of the second order Legendre polynomial $P_2(\cos\theta)$,

$$F_2(t) = \frac{\langle P_2(\cos(\theta(0)))P_2(\cos(\theta(t)))\rangle}{\langle P_2(\cos(\theta(0)))P_2(\cos(\theta(0)))\rangle}. \tag{2}$$

Throughout this contribution, the pointed brackets denote an ensemble average.

^{2}H SLR analysis provides access to the spectral density $J_2(\omega)$, which is related to the correlation function $F_2(t)$ via Fourier transformation. In these studies, it is exploited that the relaxation time T_1, which describes the buildup of ^{2}H magnetization $M(t)$, depends on the spectral density $J_2(\omega)$ of isotropic reorientation according to [18]

$$\frac{1}{T_1} = \frac{2}{15}\delta^2(J_2(\omega_0) + 4J_2(2\omega_0)) \tag{3}$$

where ω_0 is the Larmor frequency. A characteristic T_1 minimum is found in temperature-dependent studies when the correlation time τ of the rotational motion is on the order of the reciprocal Larmor frequency $\tau = 0.616\,\omega_0^{-1}$.

For complex molecular dynamics, the correlation function $F_2(t)$ deviates from a single exponential and the spectral density $J_2(\omega)$ does not show the corresponding Lorentzian shape. In our case of water in silica confinement, we apply the Cole–Cole spectral density [19]

$$J_{CC}(\omega) = \frac{\omega^{-1}\sin\left(\frac{\pi}{2}\beta_{CC}\right)(\omega\tau_{CC})^{\beta_{CC}}}{1 + 2\cos\left(\frac{\pi}{2}\beta_{CC}\right)(\omega\tau_{CC})^{\beta_{CC}} + (\omega\tau_{CC})^{2\beta_{CC}}} \tag{4}$$

which was observed in BDS studies [11, 16] and used in previous ^{2}H SLR approaches to such systems [13, 14]. The Cole–Cole spectral density is characterized by the time constant τ_{CC} and the width parameter β_{CC}. A characteristic mean correlation time τ_p can be obtained from the peak position ω_p of the corresponding dynamic susceptibility, yielding $\tau_p = 1/\omega_p = \tau_{CC}$.

When deuteron species with different dynamical behaviors coexist, ^{2}H magnetization can build up in several non-exponential relaxation steps. To consider this effect, we analyze the buildup curves, if necessary, by fitting to a sum of Kohlrausch-Williams-Watts (KWW) functions:

$$M(t) = M_\infty - \sum_x M_x \exp\left[-\left(\frac{t}{T_{1,x}}\right)^{\beta_{1,x}}\right] \tag{5}$$

Here, M_∞ is the sum of the equilibrium magnetizations M_x of the dynamically distinguishable deuteron species x. Moreover, $T_{1,x}$ and $\beta_{1,x}$ denote the time constants and stretching parameters of the individual relaxation steps, respectively. Then, the corresponding mean ^{2}H SLR times can be calculated according to $\langle T_{1,x}\rangle = (T_{1,x}/\beta_{1,x})\Gamma(1/\beta_{1,x})$, where $\Gamma(x)$ is the Gamma function.

In ^{2}H LS analysis, we exploit that the spectra of confined water show a crossover from a broad Pake pattern to a narrow Lorentzian line when the correlation time crosses the time scale of this experiment, $\tau \approx \delta^{-1} \approx 1$ µs [3]. When the ^{2}H NMR spectra are recorded using a solid echo, this LS transition is accompanied by a reduced echo intensity. When broad distributions of correlation times $G(\log \tau)$ exist, the spectra are approximately described by weighted superpositions of Pake and Lorentzian components in certain temperature ranges [20], reflecting the slow ($\tau \gg \delta^{-1}$) and fast ($\tau \ll \delta^{-1}$) parts of this distribution, respectively.

^{2}H STE experiments are sensitive to slow molecular dynamics with correlation times on the order of milliseconds. Here, we apply the Zeeman order three-pulse sequence (90°–t_p–90°–t_m–90°–t_p) to correlate the quadrupolar frequencies ω_Q during two short evolution times t_p separated by a longer mixing time t_m. Specifically, variation of the mixing time in this pulse sequence provides access to the correlation function [17, 20]

$$F_2^{cc}(t_m) \propto \langle \cos[\omega_Q(0)t_p]\cos[\omega_Q(t_m)t_p]\rangle \tag{6}$$

The angular resolution of this experiment is determined by the evolution time. It is higher for larger values of t_p. Therefore, information about the geometry of the reorientation process is available from comparison of correlation functions $F_2^{cc}(t_m)$ for various evolution times t_p [20, 21].

For an analysis of ^{2}H STE data, it is necessary to consider that, in addition to water reorientation, spin relaxation can damp the observed signal. Therefore, we fit the normalized STE decays to

$$F_2^{cc}(t_m) = \left[(1-F_\infty)\exp\left(-\left(\frac{t_m}{\tau_K}\right)^{\beta_K}\right) + F_\infty\right]\Phi(t_m) \tag{7}$$

Thus, a KWW function with a time constant τ_K and a stretching parameter β_K is used to model the decay due to water reorientation and F_∞ is introduced

to consider a possible residual correlation. Furthermore, SLR damping is described by $\Phi(t_m)$, as obtained from the concomitant SLR analysis. For straightforward comparison with results from BDS, we use the KWW fit parameters to calculate the peak times τ_p of the corresponding susceptibility maxima according to [22]:

$$\tau_p = (1.7851 - 0.87052\beta_K - 0.028836\beta_K^2 + 0.11391\beta_K^3)\tau_K \quad (8)$$

To obtain Eq. (8), the susceptibilities of KWW functions for a given τ_K and various β_K were calculated via numerical Fourier transformation, the peak positions ω_p were determined, and the corresponding correlation times $\tau_p(\beta_K)$ were interpolated with a third-order polynomial, yielding deviations by less than 0.05% from the numerical values in the range $0.05 \leq \beta_K \leq 1$.

3 Experimental

3.1 Sample preparation

MCM-41 was synthesized based on a method of Grünberg et al. [23]. 8.95 g (0.14 eq.) of dodecyltrimethylammonium bromide were dissolved in 538 mL deionized water. The mixture was heated to 35 °C (308 K) and 46.8 mL ammonia solution (25%) were added. The solution was stirred for another 90 min. Then, 45.12 g (1.00 eq.) tetraethoxysilane (TEOS) were slowly added. After the addition was complete, the suspension was stirred for 1 h. The suspension was transferred into a Teflon bottle and aged at 80 °C (353 K) for 72 h. After aging the white precipitate was filtered off. The solid was washed with deionized water and the leftover template was removed at 650 °C (923 K).

MCM-41 was functionalized using a method adapted from Adamczyk et al. [24]. 3.00 g of MCM-41 were dried under vacuum at 160 °C (433 K) over night. After cooling to room temperature, 50 mL of dry toluene and 3.20 g of APTES were added. The suspension was heated to 80 °C (353 K) and stirred for 3 h. The solid was filtered off and washed with diethyl ether. Impurities were removed using soxhlet extraction with dichloromethane over night. The product was dried under vacuum.

The samples for the ^{2}H NMR and BDS measurements were prepared by completely filling the pores of the obtained functionalized MCM-41 APTES with D_2O, as described in more detail in another contribution to this issue [25].

3.2 BET, NMR, and BDS measurements

BET measurements were carried out using model Surfer by Thermo Fisher Scientific. The samples were dried for 2 days in vacuum using a turbomolecular pump (10^{-6} mbar) at 50 °C (323 K). Nitrogen was used as measurement gas while the sample was cooled using liquid nitrogen.

MAS NMR measurements were carried out at room temperature on a Bruker AVANCE II+ spectrometer at 400 MHz proton resonance frequency, employing a Bruker 4 mm double resonance probe. Measurements were performed using a 30° pulse, a delay time of 10 s, and a MAS spinning rate of 10 kHz.

^{2}H NMR experiments on static samples were carried out on a home-built spectrometer at a Larmor frequency of $\omega_0/(2\pi) = 46.1$ MHz. The temperature was set using a Konti cryostat from CryoVac and a TIC 304 MA CryoVac temperature controller. The temperature accuracy was better than ±1 K and the temperature stability better than ±0.5 K. The duration of the 90° pulses was in the range 2.1–2.5 μs. For ^{2}H SLR and LS experiments, we applied a saturation pulse sequence followed by a solid echo detection. An interpulse delay of 20 μs was used in the solid echo. In the ^{2}H STE studies, appropriate phase cycling was employed to cancel out unwanted coherences [26].

BDS experiments were performed utilizing a Novocontrol Alpha-N High Resolution Dielectric Analyser. The sample temperature was controlled by a Novocontrol Quatro Cryosystem with an accuracy of ±0.5 K and stability better than ±0.2 K. To obtain characteristic correlation times, we determine the positions ω_p of the maxima of the dielectric susceptibility and use $\tau_p = 1/\omega_p$.

4 Results and discussion

4.1 MAS NMR and BET studies of surface modification

To follow the success of APTES modification, we use MAS NMR. Inspecting the ^{29}Si MAS spectrum of unmodified MCM-41 in Figure 1, Q2, Q3, and Q4 species are found from –92 to –112 ppm. After chemical modification, Q2, Q3 and Q4 groups are still present, but the peak intensity of the Q4 species increased in comparison to that of the other species due to condensation reactions. Furthermore, the modified material shows signals from T2 and T3 groups at –60 and –66 ppm, indicative of covalent Si–C bonds between the silica surface and the linker molecules.

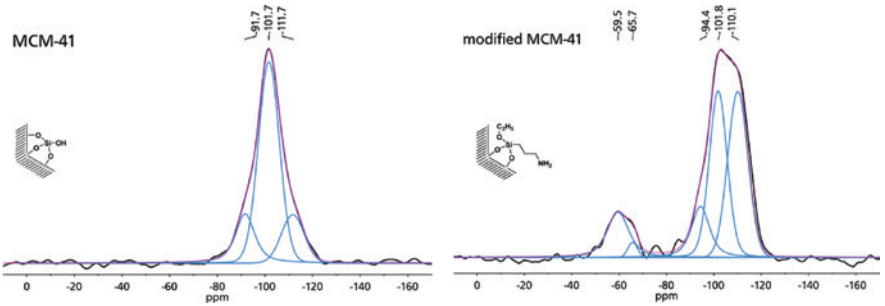

Fig. 1: ^{29}Si MAS NMR spectra of (left) unmodified MCM-41 and (right) APTES modified MCM-41 at a spinning rate of 10 kHz. In both panels, the experimental spectrum (black line) is shown together with a deconvolution into various signal contributions (blue) and their sum (pink).

Furthermore, ^{13}C CP/MAS spectra were recorded for MCM-41 APTES. In Figure 2, we see several signals between 8 and 66 ppm. The peaks at 8.7, 24.3, and 43.5 ppm can be assigned to the three carbon atoms of the linker. The additional peaks at 16.8 and 59.7 ppm belong to not fully condensed ethoxy groups of the used APTES linker. Finally, the peak at 65.4 ppm is due to surface-associated or cross-linked species of the linker.

The BET gas adsorption method was utilized to determine the pore sizes of the MCM-41 compounds. A change in the location of the hysteresis is observed when comparing the BET isotherms of the unmodified and modified materials in Figure 3. APTES modification results in a shift of the hysteresis to lower relative

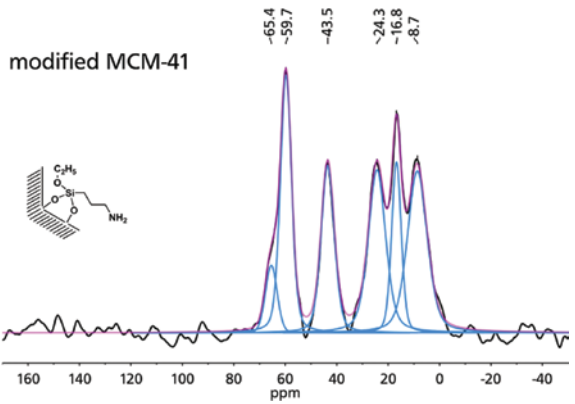

Fig. 2: ^{13}C CP/MAS NMR spectrum of MCM-41 APTES at a spinning rate of 10 kHz (black), The experimental spectrum (black line) is shown together with a deconvolution into various signal contributions (blue) and their sum (pink).

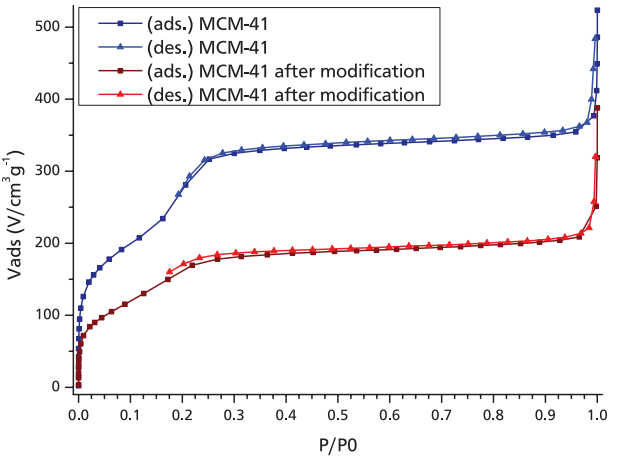

Fig. 3: Nitrogen isotherms of unmodified MCM-41 (blue) and APTES modified MCM-41 (red) at –196 °C (77 K).

pressures P/P_0, indicating a reduction of the pore diameter. Specifically, analysis of the isotherms shows that the pore diameter decreases from $d = 2.4$ nm for the unmodified MCM-41 to $d = 2.2$ nm for the modified one.

4.2 ^{2}H NMR and BDS studies of water reorientation

^{2}H NMR provides access to D_2O reorientation in MCM-41 matrices [13–15]. In the following, we compare new results for MCM-41 APTES with previous findings for unmodified MCM-41 C10 [13]. First, we perform ^{2}H SLR analysis. Figure 4 shows the build-up of magnetization $M(t)$ in the modified pores at two characteristic temperatures. While the build-up curves are monoexponential above $T \approx 210$ K, they are bimodal below this temperature with a short-time relaxation step, which continues the high-temperature behavior, and a long-time relaxation step, which emerges upon cooling. Comparable results were obtained for unmodified MCM-41 C10 [13] and other mesoporous silica [14]. There, the bimodality was rationalized by a coexistence of liquid and solid water fractions due to partial freezing. Specifically, the fast relaxation process was attributed to unfreezable water near the pore walls, while the slow relaxation process was assigned to solid water forming in the pore centers when the temperature is decreased.

The temperature-dependent mean ^{2}H SLR times $\langle T_1 \rangle$ of both water fractions are presented in Figure 5. First, we focus on the fast relaxation step. It is monoexponential ($\beta_1 \approx 1$) at $T > 180$ K so that $\langle T_1 \rangle = T_1$. A crossover to nonexponential SLR

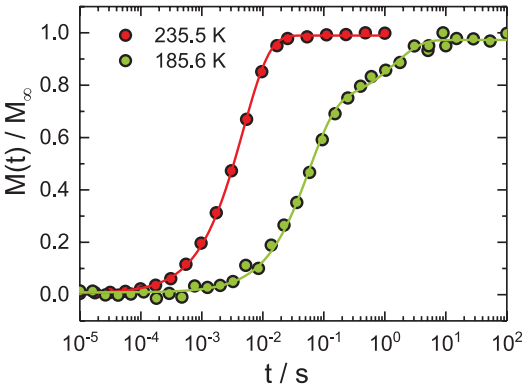

Fig. 4: Recovery of ^{2}H magnetization $M(t)$ after saturation for D_2O in MCM-41 APTES at two characteristic temperatures. The lines are fits with Eq. (5). While the build-up is monoexponential at 235.5 K, it involves two relaxation steps at 185.6 K.

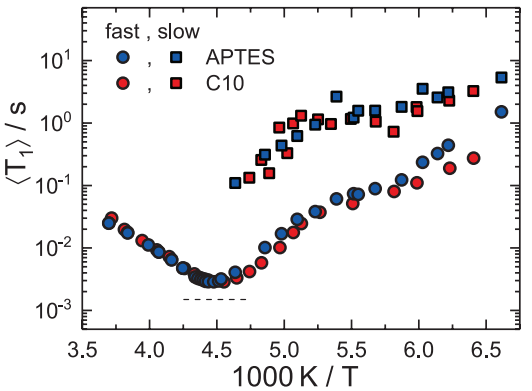

Fig. 5: Temperature-dependent mean ^{2}H spin-lattice relaxation times $\langle T_1 \rangle$ for D_2O in MCM-41 APTES and in MCM-41 C10 [13]. For both samples, two relaxation steps are distinguishable below 210–225 K, but not above this temperature range. The dashed line marks the minimum value for a Lorentzian shape of the spectral density.

occurs only at lower temperatures. For both modified and unmodified [13] MCM-41, the fast step and, hence, the dynamics of the liquid fraction is characterized by a T_1 minimum at 220–225 K, indicating a correlation time of $\tau = 0.616/\omega_0 \approx 2 \cdot 10^{-9}$ s. Hence, water dynamics in both confinements are comparable at these temperatures. The T_1 values at these minima differ from the expectation for a Lorentzian spectral density. Therefore, we use the Cole–Cole spectral density to model the heterogeneous nature of water dynamics in nanoscopic confinements. Then,

the value of the width parameter β_{CC} can be determined from the height of the T_1 minimum. For both samples, $\beta_{CC} \approx 0.6$ is obtained, implying that broad distributions of correlation times $G(\log \tau)$ exist. At temperatures below the minimum, T_1 is slightly longer for MCM-41 APTES than for MCM-41 C10 [13]. At such temperatures, longer T_1 values imply slower dynamics and, hence, this finding suggests that APTES modification results in a mild slowdown of water reorientation. The observation that the fast relaxation step is exponential although a broad distribution $G(\log \tau)$ exists reveals that the related water molecules explore a substantial part of the pore volume so that the related exchange between sites with different dynamical behaviors restores ergodicity on the timescale of T_1 [13–15], as expected for a liquid. However, when cooling through ~180 K, SLR becomes nonexpontial and its temperature dependence becomes weaker. We will return to these findings below. The slow relaxation step is nonexponential ($\beta_1 \approx 0.6$), independent of temperature. Hence, the associated water molecules do not sample diverse environments on the SLR time scale of ~1 s, i.e. they are solid. The $\langle T_1 \rangle$ values of this solid component do not differ in MCM-41 APTES and MCM-41 C10 [13].

We move on to ^{2}H LS analysis. As expected when liquid dynamics slows down upon cooling, the ^{2}H NMR solid-echo spectra of D_2O in modified and unmodified [13, 14] MCM-41 matrices evolve from a narrow Lorentzian line at high temperatures to a Pake spectrum at low temperatures. This line-shape transition is accompanied by a minimum intensity of the solid-echo signal at the corresponding intermediate temperatures. For MCM-41 APTES, we find that this minimum is located at $T = 195$ K. It occurs when water reorientation takes place on the time scale of the reciprocal spectral width, corresponding to a mean correlation time of $\tau_p = 10^{-6}$ s [27]. For MCM-41 C10, the minimum was found at a similar temperature of $T = 193$ K [13, 14], indicating comparable, possibly slightly faster water dynamics in the unmodified pore.

Figure 6 displays ^{2}H NMR solid-echo spectra of D_2O in modified and unmodified [13, 14] MCM-41 during the line-shape transition. The spectra of both samples are composed of broad and narrow spectral components. Previously, detailed analyses [13, 14] showed that this two-component line shape is a consequence of a broad distribution $G(\log \tau)$. Specifically, the broad and narrow lines can be attributed to the slow ($\tau \gg \delta^{-1}$) and fast ($\tau \ll \delta^{-1}$) parts of this distribution, respectively. Closer inspection of the shape of the motionally narrowed component reveals differences between the samples. While a narrow Lorentzian line was observed throughout the line-shape transition in unmodified MCM-41 [13, 14], the motionally narrowed component has a box-like shape with a width of about 40 kHz below ~200 K and only further narrows into a Lorentzian line when heating above this temperature in MCM-41 APTES. The latter observations resemble previous findings in ^{2}H LS analysis for myoglobin hydration water [28, 29].

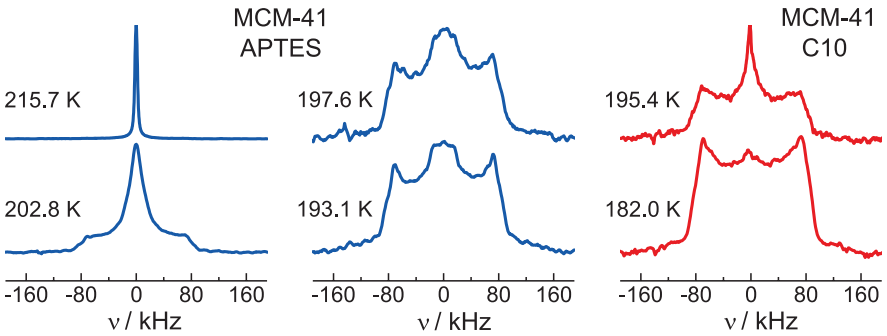

Fig. 6: ^{2}H NMR solid-echo spectra of D_2O in (left and middle) MCM-41 APTES and (right) MCM-41 C10 at the indicated temperatures.

There, line-shape simulations showed that the box-like spectral pattern can be rationalized by anisotropic large-angle motion, which only partially averages the quadrupolar interactions of the deuterons. Therefore, our results imply that D_2O reorientation in MCM-41 APTES is anisotropic on the experimental time scale of 10^{-6} s below 200 K, where the box-like pattern is found, and becomes isotropic on this time scale only at higher temperatures, where the crossover to the Lorentzian line is observed. However, at present, we cannot exclude signal contributions from deuterons that arrived at the amide group of the APTES linker due to deuteron exchange with D_2O.

Finally, we perform ^{2}H STE studies to determine the correlation time and the motional mechanism of slow water reorientation in MCM-41 APTES at low temperatures. In Figure 7a, we see that the correlation functions $F_2^{cc}(t_m)$ for an

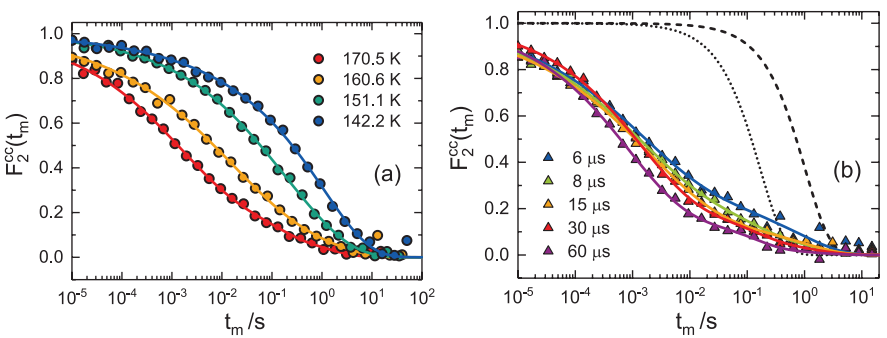

Fig. 7: $F_2^{cc}(t_m)$ for D_2O in MCM-41 APTES: (a) correlation functions at various temperatures for an evolution time of $t_p = 8$ µs and (b) correlation functions for various evolution times at $T = 170.5$ K. The lines are fits with Eq. (7). In panel (b), the dashed and dotted lines mark SLR damping $\Phi(t_m)$ associated with the fast and slow relaxation steps of the above SLR study.

evolution time of $t_p = 8$ µs shift to longer times when the temperature is decreased, indicating the slowdown of water reorientation. Moreover, they are substantially stretched, consistent with pronounced heterogeneity of water dynamics. In Figure 7b, we show $F_2^{cc}(t_m)$ for various evolution times t_p and, hence, diverse angular resolution at $T = 170.5$ K. We see two-step decays, with short-time and long-time decays due to D_2O reorientation and SLR damping, respectively. While the height of the intermediate plateau, i.e. the residual correlation F_∞, see Eq. (7), depends on the length of the evolution time, the time scale of the decays does not.

For quantitative analysis, we fit the STE data to Eq. (7). Figure 8 displays the evolution-time dependence of the obtained time constants τ_K and residual correlations F_∞ characterizing water dynamics at several temperatures. While τ_K is essentially independent of t_p, F_∞ decreases with increasing t_p at short evolution times and levels off at longer ones. The stretching parameter has nearly the same value of $\beta_K \approx 0.35$ in all measurements (not shown).

The dependence of the time scale of the correlation loss on the angular resolution of the experiment yields insights into the angles of rotational jumps [20, 21]. While the time scale strongly depends on the value of t_p for small-angle jumps, e.g. it scales as t_p^{-2} in the limit of isotropic rotational diffusion, it is essentially independent of t_p for large-angle jumps such as random or tetrahedral jumps. Thus, our finding of evolution-time independent values of τ_K and β_K shows that the motional mechanism of the reorientation dynamics is dominated by elementary jumps about large rather than small angles, consistent with previous results for low-temperature water dynamics in various environments [13–15, 27, 29, 30].

The residual correlation F_∞ yields insights into the overall geometry of the reorientation [21]. It is moderate, but higher than expected for isotropic reorientation.

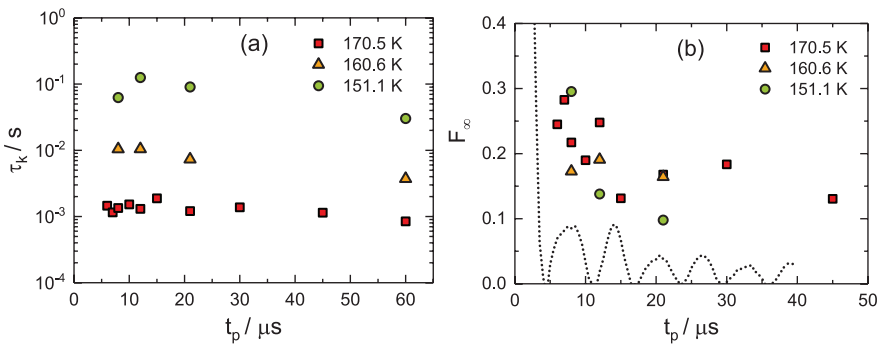

Fig. 8: Results from fits of $F_2^{cc}(t_m)$ data for D_2O in MCM-41 APTES with Eq. (7): evolution-time dependence of (a) time constants τ_K and (b) residual correlations F_∞ at the indicated temperatures.

Part of this residual correlation results from the fraction of solid water observed in the above SLR study. Considering that solid water shows very slow dynamics at the relevant temperatures, this species and any other immobile deuteron species should yield a STE contribution, which is independent of t_m and t_p. Therefore, we expect that the existence of a fraction of solid water causes the constant residual correlation of $F_\infty \approx 0.15$ at long evolution times, while information about the fraction of liquid water is available from the variation at smaller values of t_p. Specifically, F_∞ grows when the evolution time is reduced in the range $t_p = 5$–20 μs, at variance with the expectation for isotropic reorientation. This observation shows that, despite an overall large amplitude, water reorientation of the liquid component is anisotropic rather than isotropic. Due to the contributions from the solid component and the interference of spin relaxation, it is, however, not possible to obtain more detailed information about the geometry of the reorientation process. Previous STE studies on the mechanism for low-temperature D_2O dynamics in unmodified MCM-41 [13, 14] and in protein matrices [27, 29] arrived at the same conclusions. Specifically, it was argued that, under such circumstances, water reorientation shows a mild anisotropy and involves large-angle rather than small angle jumps. As a possible motional model, distorted tetrahedral jumps were proposed.

A combination of the ^{2}H SLR, LS, and STE results allows us to determine correlation times for the rotational motion of confined water in a wide dynamic range of more than 10 orders of magnitude. In Figure 9, we show the ^{2}H NMR mean correlation times τ_p of D_2O reorientation in MCM-41 APTES together with

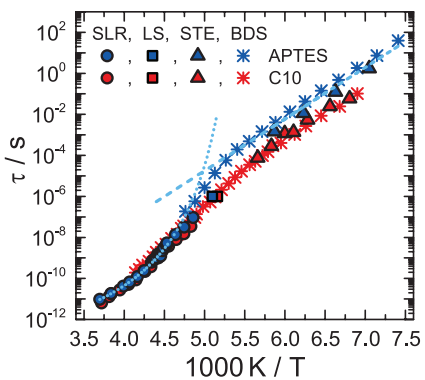

Fig. 9: Temperature-dependent correlation times τ_p for D_2O in MCM-41 APTES and in MCM-41 C10 [13]. ^{2}H NMR data from SLR (circles), LS (squares) and STE (triangles) analyses are compared with BDS results from present studies on D_2O in the APTES modified sample and previous findings for H_2O in MCM-41 C10 [16]. The ^{2}H NMR correlation times obtained for MCM-41 APTES are fitted to a VFT behavior (dotted line) for high *T* and to an Arrhenius law (dashed line) for low *T*.

that in MCM-41 C10 [13]. For both samples, the temperature dependence can be well described by a Vogel-Fulcher-Tammann (VFT) behavior

$$\tau_p = \tau_0 \exp\left(\frac{B}{T - T_0}\right) \tag{9}$$

at temperatures above 210–225 K and by an Arrhenius law

$$\tau = \tau_0 \exp\left(\frac{E_a}{k_B T}\right) \tag{10}$$

with an activation energy of $E_a = 0.5$ eV at temperatures below 180–185 K. In the whole temperature range, the ^{2}H NMR data are in harmony with BDS correlation times from present studies on D_2O in MCM-41 APTES and previous work on H_2O in MCM-41 C10 [16].

The high-temperature range is limited by a first dynamic crossover at ~210 K and ~225 K for modified and unmodified [13] MCM-41, respectively. Near these temperatures, a solid water species forms in these confinements, see Figure 5, resulting in a reduction of the pore volume accessible to the liquid water species. Therefore, we conclude, consistent with previous arguments [13–15], that the first dynamic crossover occurs when the liquid component becomes sandwiched between solid water and silica walls and, hence, its dynamics becomes interface-dominated. A second dynamic crossover marks the onset of the low-temperature Arrhenius regime upon cooling through 180–185 K. Near these temperatures, ^{2}H SLR shows a bending in the temperature dependence, see Figure 5, and it changes from exponential ($\beta_1 = 1$) to stretched ($\beta_1 < 1$) behavior. For bulk and confined glass-forming liquids, these effects are observed when the glass transition temperature T_g is crossed [31, 32]. Therefore, we follow previous works [4, 13–15] and propose that the second dynamic crossover is an indirect consequence of a dynamic arrest resembling a glass transition. Specifically, consistent with the anisotropy of the probed motion, we argue that the observed correlation times do not characterize the structural (α) relaxation of severely confined water, but its secondary (β) relaxation, which usually shows a kink in the temperature dependence when ergodicity is broken at T_g [12, 33].

5 Conclusion

The inner surfaces of mesoporous silica MCM-41 were functionalized using 3-(aminopropyl)triethoxysilane (APTES). Successful chemical bonding was dem-

onstrated by changes in ^{13}C and ^{29}Si MAS NMR spectra and in BET isotherms. The obtained APTES modified MCM-41 has a pore diameter of $d = 2.2$ nm.

^{2}H NMR proved well suited to investigate D_2O reorientation in MCM-41 APTES. Specifically, the combination of ^{2}H SLR, LS, and STE studies provided access to broad dynamic and temperature ranges. A change from monomodal to bimodal SLR revealed that, most probably due to partial crystallization, a solid water species emerges upon cooling through ~210 K and coexists with a liquid water species below this temperature. These NMR approaches were complemented by BDS measurements on D_2O in MCM-41 APTES.

Our studies consistently showed that the reorientation dynamics of the liquid water species is characterized by pronounced dynamical heterogeneity in the whole temperature range. For example, a Cole–Cole spectral density with a width parameter $\beta_{CC} = 0.6$ described the SLR data at high temperatures and a KWW function with a stretching parameter $\beta_K \approx 0.35$ characterized the STE data at low temperatures. However, the emergence of the solid water species affected the temperature dependence of the correlation times of the liquid water species. We did not interpret the mild dynamic crossover from a higher to a lower temperature dependence at ~210 K in terms of a fragile-to-strong transition related to a liquid-liquid phase transition. Rather, we argued that the formation of a solid water phase further restricts the volume accessible to the liquid water phase, leading to even more pronounced deviation from bulk-like behavior towards interface-dominated dynamics. Moreover, combined SLR and STE studies provided evidence that, at low temperatures, the NMR correlation times, just as the BDS data, do no longer probe the structural (α) relaxation of confined liquid water, but a secondary (β) relaxation associated with an anisotropic water reorientation, which involves large-angle jumps, possibly, distorted tetrahedral jumps. Another mild dynamic crossover occurs when the temperature-dependence of this secondary relaxation changes. This effect is best seen in the BDS results, which are fully consistent with the NMR findings in the whole common temperature range. SLR analysis implied that this crossover of the secondary relaxation occurs in response to a dynamic arrest of the structural relaxation during a glass transition of interfacial water at ~180 K. The α relaxation is otherwise unobserved by methods probing rotational dynamics, such as NMR and BDS, possibly, due to the fact that, as consequence of its exceptionally large rotational amplitude, the faster β process destroys most orientational correlation prior to the action of the slower α process. However, positron annihilation lifetime spectroscopy provided evidence for a glass transition of interfacial water in this temperature range [34]. For temperatures below the second dynamic crossover, we found that the correlation times obey an Arrhenius law with an activation energy of $E_a = 0.5$ eV.

Comparing present and previous results, we observed that D_2O shows similar reorientation dynamics in modified MCM-41 APTES and in unmodified MCM-41 C10, which have comparable pore diameters of $d = 2.2$ nm and $d = 2.1$ nm, respectively. In particular, in ^2H NMR work on D_2O in MCM-41 C10 [13], two dynamic crossovers at similar temperatures of ~225 K and ~185 K were also attributed to a formation of crystalline and glassy water species. Moreover, although low-temperature water dynamics is almost an order of magnitude slower in the modified than in the unmodified confinement, it is characterized by the same activation energy of $E_a = 0.5$ eV in both samples. These similarities indicate that APTES modification hardly alters the dynamical properties of water. On the other hand, ^2H NMR studies [14, 22] on D_2O in various mesoporous silica reported that water dynamics can significantly depend on the pore diameter. Specifically, when the confinement size is reduced, deviations from Arrhenius behavior become weaker in the high-temperature regime above the first crossover, where the structural relaxation is observed, while the common activation energy of $E_a = 0.5$ eV remains unaffected in the low-temperature range below the second crossover, where a secondary relaxation is probed. Most probably, this common low-temperature activation energy corresponds to the energy to break at least two hydrogen bonds in the network formed near solid surfaces.

In conclusion, confinement affects various dynamical modes of water differently. The high-temperature α process depends strongly on the size of the geometrical restriction, but only weakly on the properties of the inner surfaces, i.e. on guest-host interactions. The low-temperature dynamics, which is most probably related to the β process, may have somewhat different correlation times in various confinements, but it shows a common activation energy of $E_a = 0.5$ eV.

Acknowledgement: Financial support of the Deutsche Forschungsgemeinschaft (DFG) in the framework of Forschergruppe FOR 1583 through grants Bu-911/18-1/2 and Vo-905/8-1/2 is gratefully acknowledged.

References

1. M. Alcoutlabi, G. B. McKenna, J. Phys.: Condens. Matter **17** (2005) R461.
2. R. Richert, Annu. Rev. Phys. Chem. **62** (2011) 65.
3. M. Vogel, Eur. Phys. J. Special Topics **189** (2010) 47.
4. S. Cerveny, F. Mallamace, J. Swenson, M. Vogel, L. Xu, Chem. Rev. **116** (2016) 7608.
5. S. Kittaka, S. Ishimaru, M. Kuranishi, T. Matsuda, T. Yamaguchi, Phys. Chem. Chem. Phy. **8** (2006) 3223.
6. S. Jähnert, F. V. Chavez, G. E. Schaumann, A. Schreiber, M. Schönhoff, G. H. Findenegg, Phys. Chem. Chem. Phys. **10** (2008) 6039.

7. J. Deschamps, F. Audonnet, N. Brodie-Linder, M. Schoeffel, C. Alba-Simionesco, Phys. Chem. Chem. Phys. **12** (2010) 1440.
8. P. Ball, Chem. Rev. **108** (2008) 74.
9. L. Liu, S.-H. Chen, A. Faraone, C.-W. Yen, C.-Y. Mou, Phys. Rev. Lett. **95** (2005) 117802.
10. P. H. Poole, F. Sciortino, U. Essmann, H. E. Stanley, Nature **360** (1992) 324.
11. J. Swenson, H. Jansson, R. Bergman, Phys. Rev. Lett. **96** (2006) 247802.
12. J. Swenson, S. Cerveny, J. Phys.: Condens. Matter **27** (2015) 033102.
13. M. Sattig, M. Vogel, J. Phys. Chem. Lett. **5** (2014) 174.
14. M. Sattig, S. Reutter, F. Fujara, M. Werner, G. Buntkowsky, M. Vogel, Phys. Chem. Chem. Phys. **16** (2014) 19229.
15. M. Rosenstihl, K. Kämpf, F. Klameth, M. Sattig, M. Vogel, J. Non-Cryst. Solids **407** (2015) 449.
16. J. Sjöström, J. Swenson, R. Bergman, S. Kittaka, J. Chem. Phys. **128** (2008) 154503.
17. K. Schmidt-Rohr, H. W. Spiess, Multidimensional Solid-State NMR and Polymers, Academic Press, London (1994).
18. N. Bloembergen, E. M. Purcell, R. V. Pound, Phys. Rev. **730** (1948) 679.
19. P. A. Beckmann, Phys. Rep. **171** (1988) 85.
20. R. Böhmer, G. Diezemann, G. Hinze, E. Rössler, Prog. Nucl. Magn. Reson. Spectrosc. **39** (2001) 191.
21. G. Fleischer, F. Fujara, NMR, Basic Principles and Progress, volume 30 of NMR, Springer Berlin Heidelberg, 1 edition (1994), P. 159.
22. D. Demuth, M. Sattig, E. Steinücken, M. Weigler, M. Vogel, Z. Phys. Chem. **232** (2018) 1059.
23. B. Grünberg, T. Emmler, E. Gedat, I. Shenderovich, G. H. Findenegg, H.-H. Limbach, G. Buntkowsky, Chem. – Eur. J. **10** (2004) 5689.
24. A. Adamczyk, Y. Xu, B. Walaszek, F. Roelofs, T. Pery, K. Pelzer, K. Philippot, B. Chaudret, H.-H. Limbach, H. Breitzke, G. Buntkowsky, Chem. Eur. J. **10** (2004) 5689.
25. M. Brodrecht, E. Klotz, C. Lederle, H. Breitzke, B. Stühn, M. Vogel, G. Buntkowsky, Z. Phys. Chem. **232** (2018) 1003.
26. D. Schaefer, J. Leisen, H. W. Spiess, J. Magn. Reson. A **115** (1995) 60.
27. M. Vogel, Phys. Rev. Lett. **101** (2008) 225701.
28. S. A. Lusceac, M. R. Vogel, C. R. Herbers, BBA-Proteins Proteom. **1804** (2010) 41.
29. S. A. Lusceac, M. Vogel, J. Phys. Chem. B **114** (2010) 10209.
30. M. Sattig, K. Elamin, M. Reuhl, J. Swenson, M. Vogel, J. Phys. Chem. C **121** (2017) 6796.
31. W. Schnauss, F. Fujara, H. Sillescu, J. Chem Phys. **970** (1992) 1378.
32. S. A. Lusceac, C. Koplin, P. Medick, M. Vogel, N. Brodie-Linder, C. LeQuellec, C. Alba-Simionesco, E. A. Rössler, J. Phys. Chem. B **108** (2004) 16601.
33. K. L. Ngai, S. Capaccioli, A. Paciaroni, Chem. Phys. **424** (2013) 37.
34. N. Roussenova, M. A. Alam, S. Townrow, D. Kilburn, P. E. Sokol, R. Guillet-Nicolas, F. Kleitz, New J. Phys. **16** (2014) 103030.